

Electrochemical Activities of Electrolytic Manganese Dioxide (EMD) as a Cathode Electrode for Lithium Air Batteries

Jinyong Shim, Hyejin Choi, Yongsug Tak*

Department of Chemical Engineering, Inha University, Incheon 402-751, Korea

*E-mail: ystak@inha.ac.kr

Received: 3 June 2015 / Accepted: 29 June 2015 / Published: 28 July 2015

Electrolytic manganese dioxide, prepared by anodic electrodeposition, was investigated for the possible application as cathode active material for lithium air battery. Electrolytic manganese dioxide showed the catalytic activity by lowering overpotentials for discharge and charge reactions. FT-IR and mass spectroscopy analysis suggested that lithium carbonates compounds were the main products formed during discharge and only a small amount of lithium oxides were produced. Furthermore, surface analysis and electrochemical impedance spectroscopy supported that discharge products were not fully removed during charge process and, that is, discharge and charge reactions were only partially reversible. Measurement of electrolytic manganese dioxide mass changes during cyclic voltammetry showed that 27.5% of discharge reduction reaction products were not removed during charge oxidation reaction. The remaining discharge products on air cathode disturbed the access of oxygen reactant to the reaction sites and deteriorated the cell performance. In order to improve the cycleability of lithium air battery, the reaction mechanism of charge-discharge reaction must be elucidated to overcome the irreversibility during cycling.

Keywords: Li-air battery, electrolytic manganese dioxide, EQCM, lithium oxide, lithium carbonate

1. INTRODUCTION

Currently, a global interest on high capacity-based new energy storage device has been greatly increased. As of now, capacity of Li-ion batteries used in all areas of our lives is approximately in the range of 130~150mAh g⁻¹[1-3]. In the fields of requiring high-capacity such as energy storage device and electric vehicle, lithium-air battery has drawn a great attraction because its theoretical capacity is several times greater than that of lithium-ion battery. Lithium-air battery can be divided into two different types according to electrolyte; aqueous-based and non-aqueous battery. When non-aqueous electrolyte is used, the active surface area of air cathode can be blocked by solid products, lithium

oxides and lithium carbonate compounds produced during discharge process, which eventually leads to a breakdown of battery by inhibiting the diffusion of air [4-7]. Furthermore, the formation of lithium carbonate compounds by the dissociation of electrolyte during discharge can result in the shortage of electrolyte which leads to the significant performance degradation of lithium air battery. In the process of charge process following discharge, facile dissociation of discharge products (Li_2O_2 , Li_2O , Li_2CO_3) must be required and MnO_2 , Co_3O_4 , and Fe_3O_4 are currently suggested as catalysts for the dissociation reaction during charge [4]. MnO_2 is not only very easily accessible and economical material, but also it has been used as a catalyst for oxygen reduction reaction in alkaline media. MnO_2 has diverse phases such as α -, β -, γ -, and δ -phase and electrochemically prepared MnO_2 (γ -phase) is called as electrolytic manganese dioxide (EMD) [8]. EMD can be prepared by anodic electrodeposition method and it has the intergrowth structure of (1 x1) tunnels of pyrolusite and (1 x2) tunnels of ramsdellite. EMD has been used as cathode active material of alkaline batteries due to its outstanding electrical activation [9-10].

In this work, EMD was used as a cathode active material for lithium air battery. EMD was directly synthesized through anodic electrodeposition method onto Ti substrate electrode and electrochemical quartz microbalance (EQCM) Pt electrode. Quantitative discussion of discharge-charge product was investigated with *in-situ* monitoring of mass changes of EMD with EQCM during cyclic voltammetry. Catalytic effects of EMD for air cathode of lithium air battery were investigated with FT-IR, SEM and TEM, and electrochemical impedance spectroscopy (EIS). In order to elucidate the deposited materials during discharge, mass spectroscopy and FT-IR was utilized for the detection of dissociation products during charge process.

2. EXPERIMENTAL

Nanostructured manganese dioxide thin films were electrodeposited at room temperature with three electrode system [11]. Prior to electrodeposition, Ti substrate electrode was mechanically polished to remove surface oxide layer and increase surface area with successive finer grade SiC papers. Polished Ti electrode was cleaned with water and ethanol solutions and used as a working electrode for the deposition of EMD. Electrolyte for the preparation of EMD was composed of 0.1M $\text{MnSO}_4 \cdot \text{H}_2\text{O}$ and 0.1M H_2SO_4 and reaction temperature is maintained at 80°C. Pt plate was used as a counter electrode and a saturated calomel electrode (SCE) was used as a reference electrode. EMD films were galvanostatically deposited with anodic current density of $50 \mu\text{A}/\text{cm}^2$ for 10min. All chemicals were purchased from Sigma Aldrich without further treatment. In-situ mass changes of electrodes during electrodeposition and the cyclic voltammetry of EMD were monitored using an electrochemical quartz crystal microbalance (QCM 917, Seiko EG&G). Sauerbrey's equation, $\Delta f = -C_f \Delta m$, was used to relate mass (Δm) and frequency change (Δf) and the constant C_f was $935.7 \text{ Hz}/\mu\text{g}$ [12].

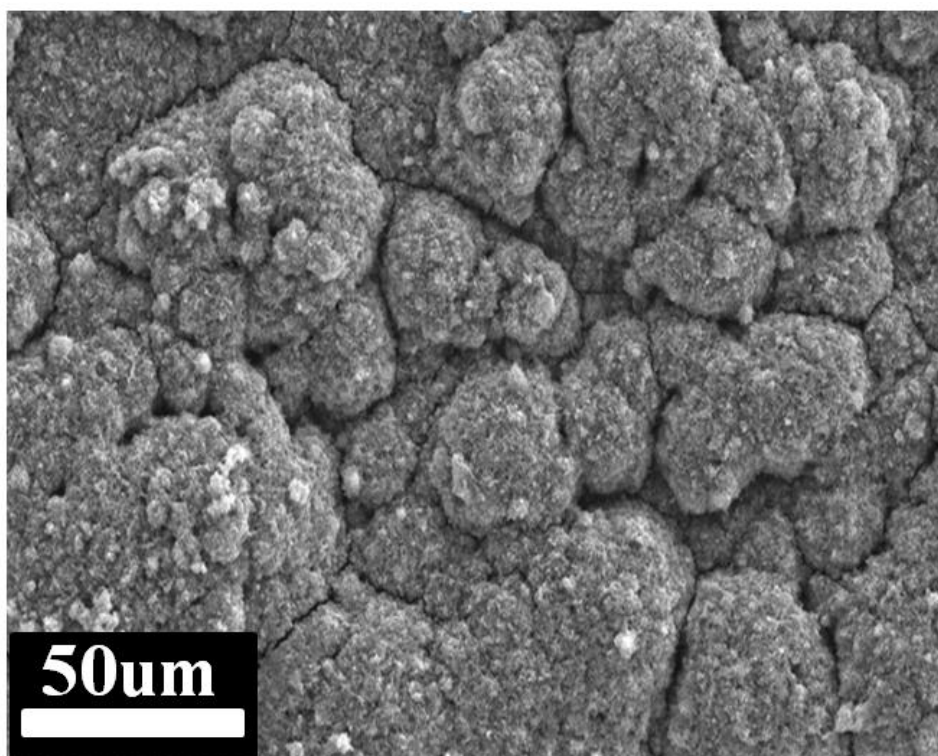
Lithium air battery for electrochemical analysis was based on a Swagelok-type Teflon container, similar to the one reported by Beattie *et al.* [13]. Cell was assembled in argon-filled glove box in which the moisture and oxygen concentration were less than 1ppm. Swagelok type lithium air

cell is composed of a lithium metal anode (Sigma Aldrich, 0.38mm), 1M LiPF₆ in propylene carbonate(PC), ethylene carbonate(EC) and diethyl carbonate(DEC) with a volume ratio (1:4:5) impregnated into a glass fiber separator (Whatman, GF/B), and a catalyzed porous air-cathode.

Catalyzed porous air-cathode was formed by casting the mixture of Ketjen black (EC600JD, Akzo Nobel, ~1420m²//g), electrolytic manganese dioxide(EMD) catalyst, and poly vinylidene fluoride as binder (Alfa Aesar) with a weight ratio (7:2:1) onto a nickel form current collector. Then, the air-cathode was dried at 110°C for several hours. For electrochemical tests, a small hole (0.4cm²) was placed on the cathode side to allow the oxygen flow. Discharge-charge cycling of the cell was done using a potentiostat/galvanostat (PGSTAT302N, Autolab) with a lower voltage limit of 2.0V and an upper limit of 4.5V vs. Li⁺/Li.

Morphologies of the electrode materials were examined using a field emission scanning electronic microscope (Hitachi, FE-SEM S-4300) and a transmission electron microscope (Philips, CM200) operating at a 200kV accelerating voltage. The crystal structures of specimen were determined by XRD (Philips X'Pert PRO MRD). Fourier transform infrared spectroscopy (FT-IR, Bruker VERTEX 80V) was applied for the characterization of materials and electrochemical impedance spectroscopy (PGSTAT302N, Autolab) was used to analyze the resistances of cell components. Quadruple Mass spectroscopy (SRS RGA 200) was used for the detection of dissociation products during charge process.

3. RESULTS AND DISCUSSION



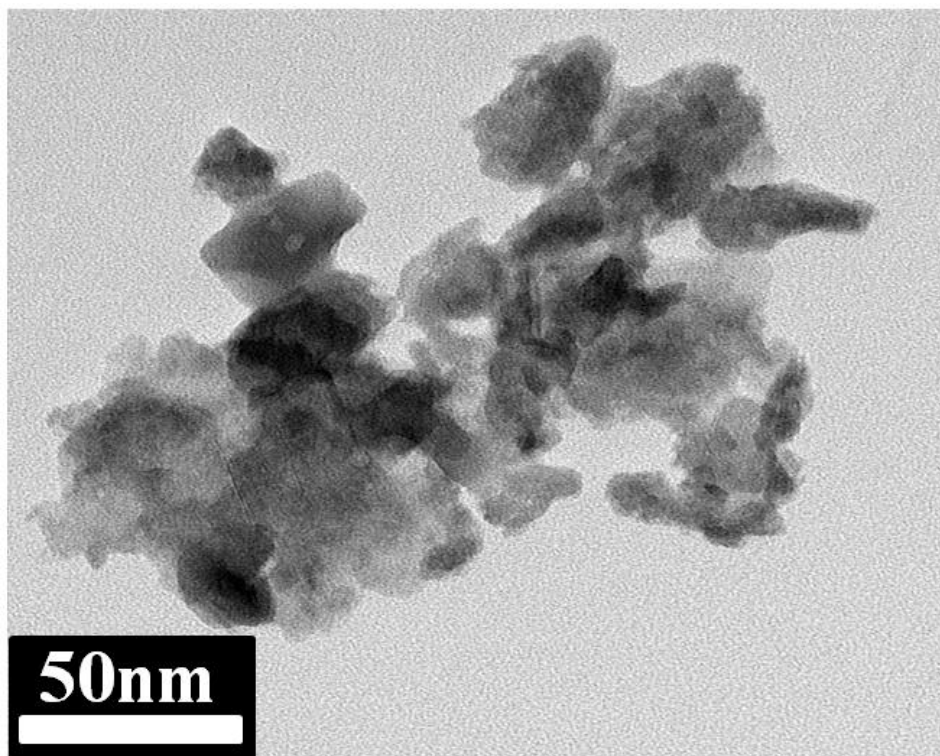


Figure 1. SEM(top) and TEM(bottom) images of electrodeposited EMD on Ti substrate. applied anodic current density: $50\mu\text{A}/\text{cm}^2$, deposition time: 10min.

Electrolytic manganese dioxide (EMD) was electrochemically prepared by applying constant anodic current of $50\mu\text{A}/\text{cm}^2$ on Ti substrate electrode.

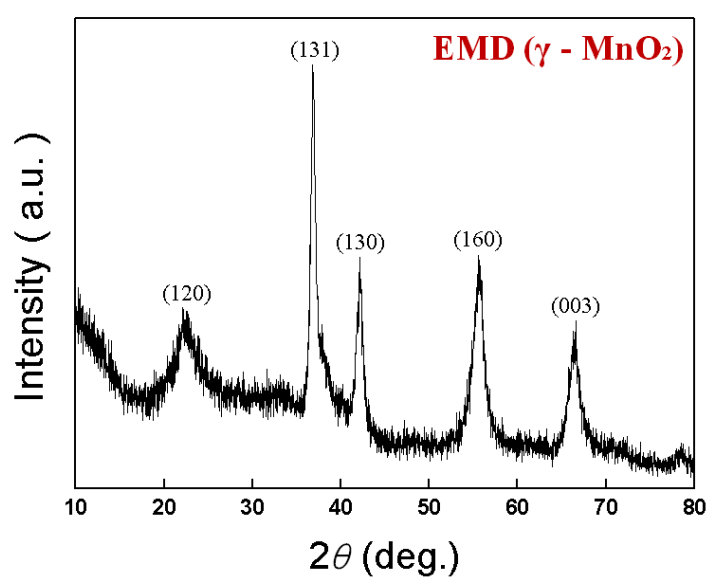


Figure 2. X-ray diffraction(XRD) pattern of as-prepared EMD. applied anodic current density: $50\mu\text{A}/\text{cm}^2$, deposition time: 10min.

Scanning electron spectroscopy (SEM) and transmission electron spectroscopy (TEM) images of EMD in Figure 1 show that 20-50 nm nanosize EMD were uniformly distributed on the Ti substrate. During the electrodeposition reaction of EMD, $Mn^{2+} + 2H_2O \rightarrow MnO_2 + 4H^+ + 2e^-$, it has been known that the formation of oxygen containing intermediate Mn(III) species (e.g., MnOOH, $[Mn(OH_2)_6]^{3+}$, and Mn_2O_3) is inevitable and these species play an important role in the morphology of EMD by the inhibition grain growth mechanism on the electrode/electrolyte interface [14-15].

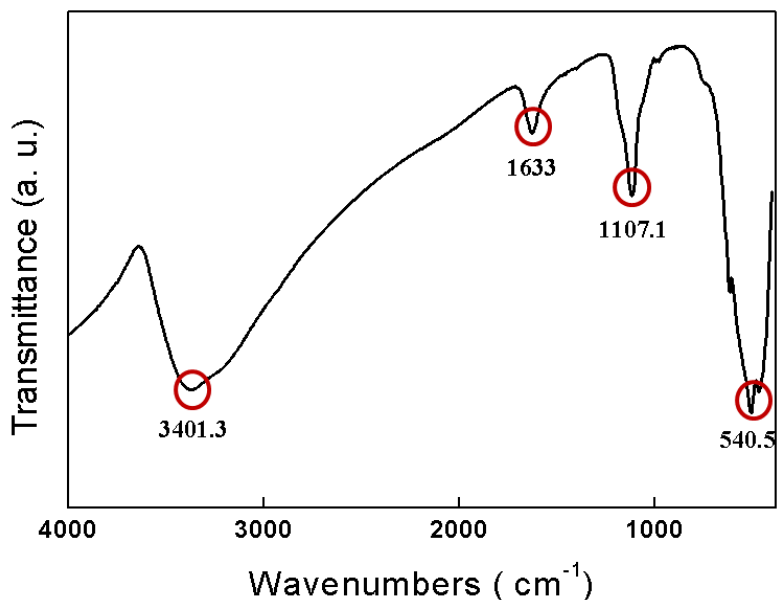


Figure 3. FT-IR spectra for as-prepared EMD. applied anodic current density: $50\mu A/cm^2$, deposition time: 10min.

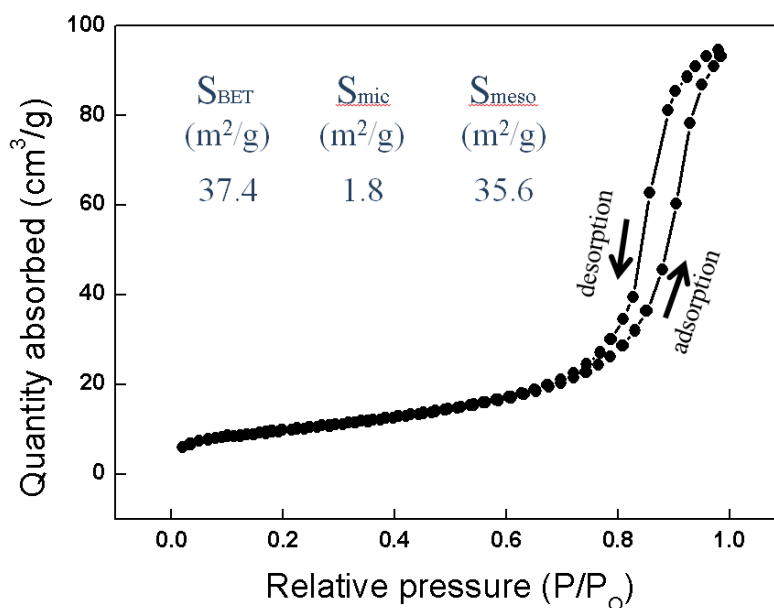


Figure 4. N₂ adsorption-desorption isotherm for as-prepared EMD. applied anodic current density: $50\mu A/cm^2$, deposition time: 10min.

Fig. 2 shows the X-ray diffraction (XRD) patterns of orthorhombic EMD. XRD peaks of EMD were assigned as 22.2° (120), 36.6° (131), 41.7° (300), 55.6° (160), 66.1° (003). All of the peaks observed can be assigned to γ - MnO_2 phase (ICDD-JCPDS No. 14-0644, $a = 6.36 \text{ \AA}$, $b = 10.15 \text{ \AA}$ and $c = 4.09 \text{ \AA}$) [16-17]. Figure 3 suggests that EMD (540.5cm^{-1}) has OH (3401.4 and 1633cm^{-1}) and sulfate (1107.1 cm^{-1}) groups that originated from electrolyte remaining on EMD [18].

Fig. 4 show the nitrogen adsorption-desorption isotherms of EMD. The isotherms of EMD are typical IV type isotherms with H1-type hysteresis loop, which is characteristic one for mesoporous materials. The BET surface area of EMD is calculated to be $37.4\text{m}^2 \text{ g}^{-1}$ and pore-size distribution calculated from the isotherm indicates that the pore size is in the range of 2 to 70nm [19].

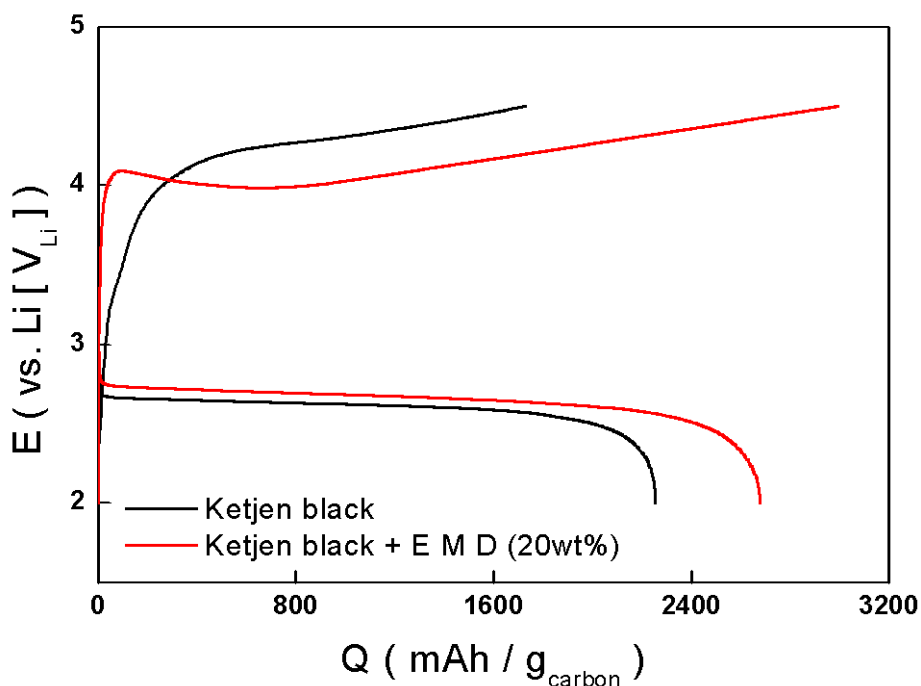


Figure 5. Variation of cell potentials during discharge-charge process of the lithium air cell. current density: $0.2\text{mA}/\text{cm}^2$.

After deposition, the electrolytic MnO_2 is mechanically removed from the electrode and ground, washed, neutralized and dried for application of lithium air battery cathode [20-21]. Electrochemical properties of the EMD were first studied by discharging-charging tests in Swagelok type cell. Fig. 5 shows the effect of MnO_2 cathode on the initial discharge-charge behaviors of lithium air battery. Compared to KB only cathode which shows the specific capacity of 2253mAhg^{-1} during discharging and 1720mAhg^{-1} during charging, cathode containing 20wt% EMD electrode has the higher capacity of 2680mAhg^{-1} , 2990mAhg^{-1} during discharging-charging process, respectively. Specific capacity of KB containing 20wt% EMD electrode is larger than pure KB electrode in both discharge and charge process. Since the capacity is based on the carbon only, the practical capacity will be lower since the mass of both binder and catalyst are included in air cathode. In case of coulombic efficiency, which is the ratio of discharging capacity to charging capacity, the KB

containing 20wt% EMD electrode of 110% is larger than pure KB electrode of 76.3%. Figure 5 also indicates that KB containing 20wt% EMD has a high discharge potential and a low charge potential than KB only cathode. It results from the electrocatalytic effect of EMD, which has a low overpotential for both the formation reaction of discharge products and the dissociation reaction of discharge products during charging process [22].

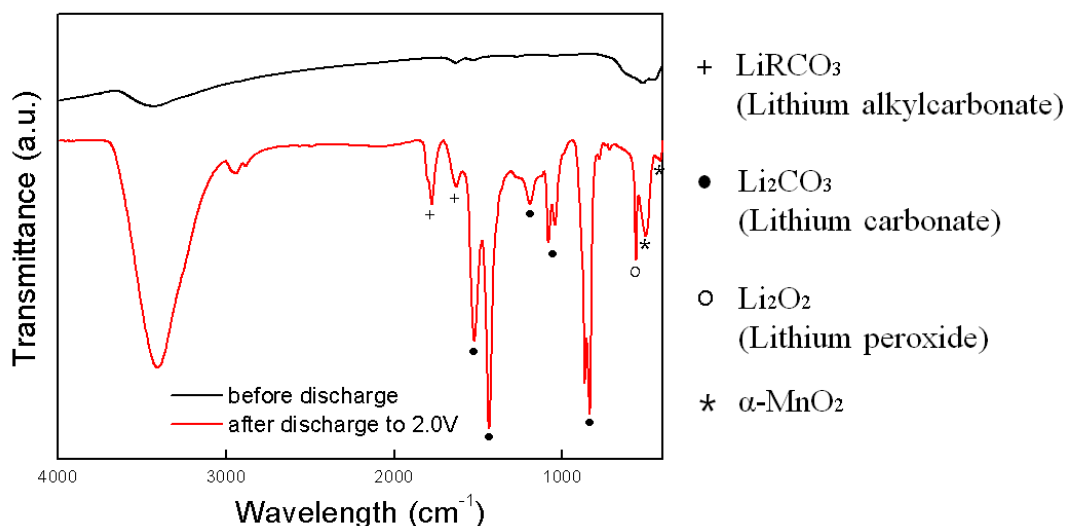


Figure 6. FT-IR analysis of air cathode after discharging to 2.0V. current density: 0.2mA/cm².

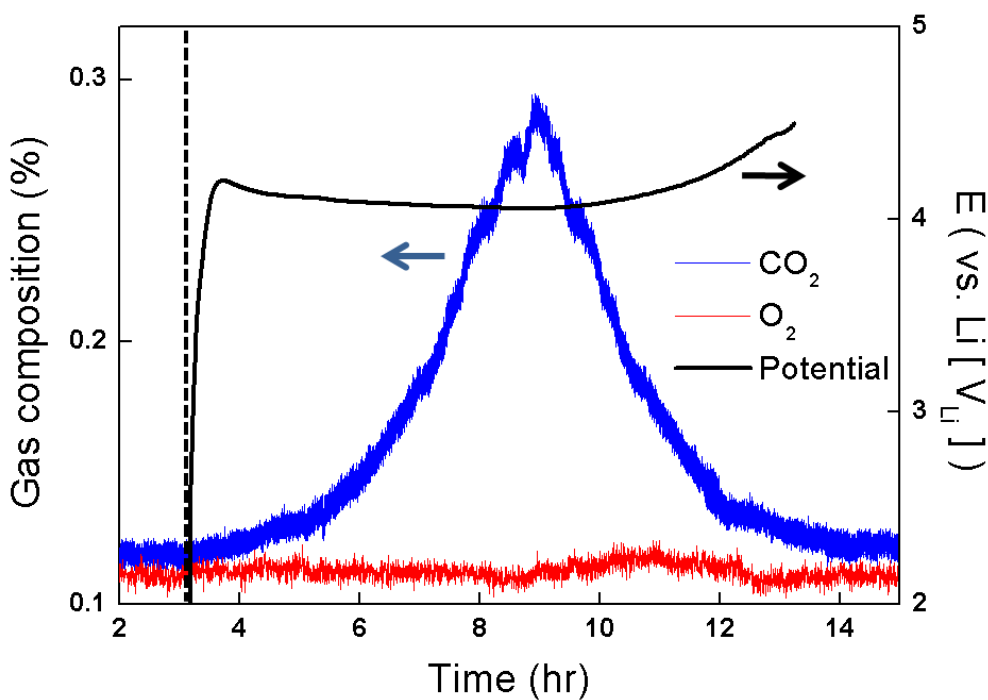


Figure 7. Mass spectroscopy of effluent from air cathode during charging process. charging current density: 0.2mA/cm².

Figure 6 shows the FT-IR analysis of cathode (α - MnO_2) after discharging to 2.0 V. Lithium carbonate, lithium alkylcarbonate, and lithium oxide (Li_2CO_3 , LiRCO_3 , Li_2O_2) are present on the electrode surface and these species are supposed to be the discharge products. Lithium carbonate compounds are originated from the decomposition of solvents in the electrolyte [23-25]. In order to elucidate the reaction mechanism during the charging process, the effluent gas composition from air electrode during charging was directly analyzed with mass spectroscopy connected to gas chromatography. Figure 7 shows that CO_2 is the main product which comes from the decomposition of various lithium carbonate compounds and the very small amount of O_2 is observed by the decomposition of lithium oxides. It supports that the main discharging products on air cathode are not lithium oxides but lithium carbonate compounds [26-27].

In order to investigate the effect of discharging on the electrochemical performance of lithium air battery, the electrochemical impedance spectroscopy (EIS) was measured and analyzed. Fig. 8 shows the Nyquist plot of the lithium air cell measured before and after the first discharge-charge cycling process in a frequency range of 100kHz - 0.03Hz. All plots are similar in shape with a broad semicircle at the high frequency range and a linear tail at the low frequency range [28].

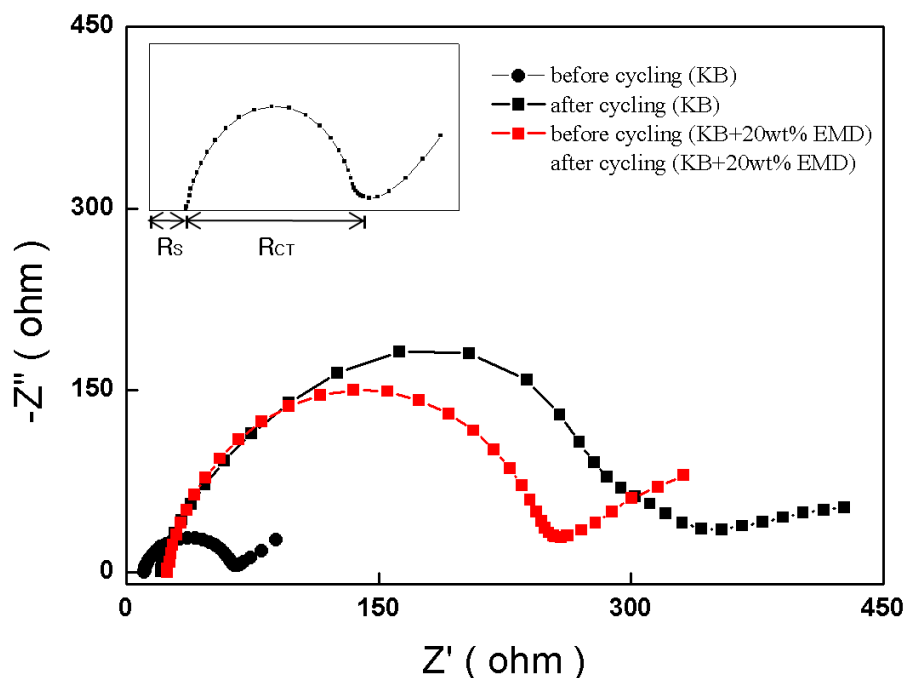


Figure 8. Electrochemical impedance spectroscopy(EIS) of the cell before and after a single cycling. Frequency range: 0.03Hz-100kHz. current density: $0.2\text{mA}/\text{cm}^2$.

SEM images in Figure 9(a) and (b) show that the surface and nanopores of air cathode was mostly covered with reaction products after cycling. FT-IR and surface analysis of air cathode clearly indicates that poor electronic conductive discharge products generated at air-cathode are not fully removed [27]. Irrespective of the MnO_2 presence, the charge-transfer (R_{CT}) and solution resistance (R_{S}) of both cells increases significantly after a single discharge-charge cycling process. However,

addition of 20% EMD results in the lower value of R_{CT} than KB only cathode. It reflects that discharge products, Li_2CO_3 , LiRCO_3 , and Li_2O_2 , are catalytically well decomposed with MnO_2 .

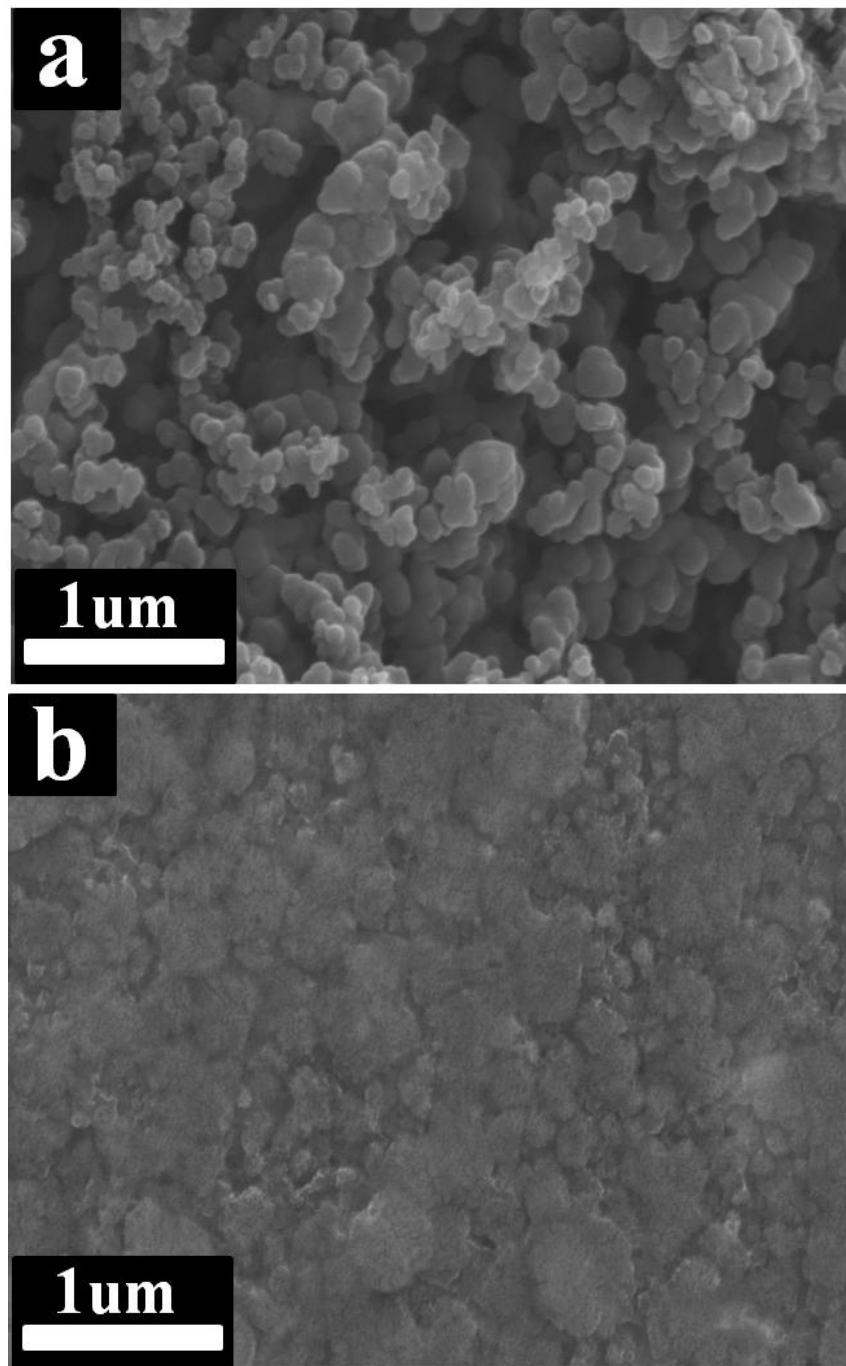


Figure 9. SEM surface images of air cathode before (a) and after (b) discharging to 2.0V. discharging current density: $0.2\text{mA}/\text{cm}^2$.

Variation of R_{CT} after a single cycling can be caused by the degradation of Li anode and air cathode. Although the Li anode was not investigated in current work, the above-mentioned results support that electrochemical behaviors of air cathode are responsible for the measured charge-transfer

resistance of the cell. Solution resistance (R_s) is also increased after a cycling but the effect of MnO_2 addition on R_s is not observed. Decomposition of electrolyte during discharging induces the decrease of electrolyte amount and the possible contamination of electrolyte with discharging products [29-31]. It is an irreversible process which increases solution resistance, R_s .

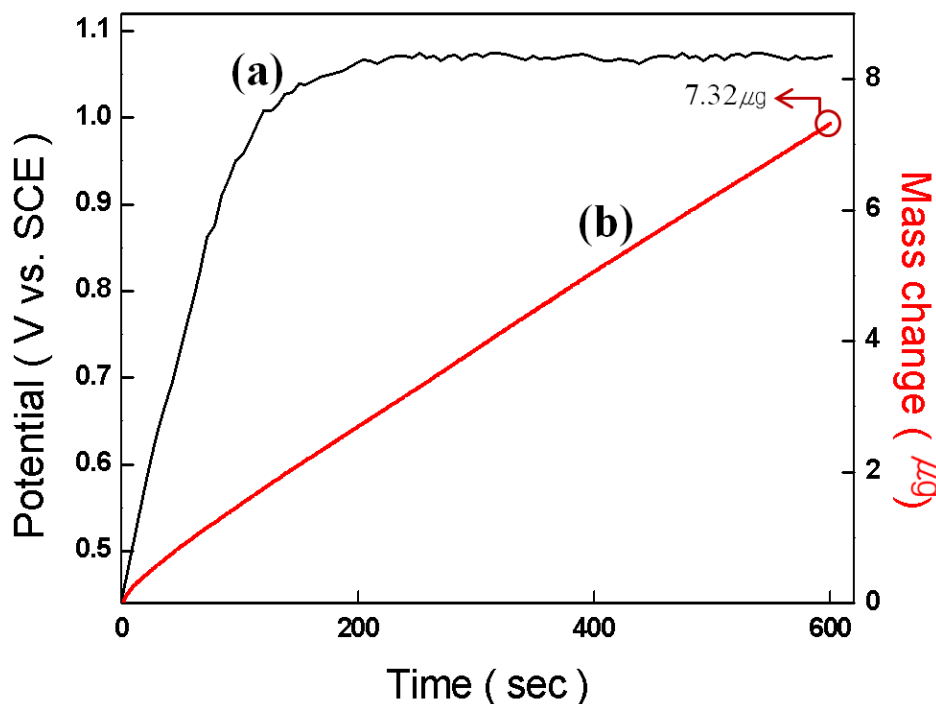


Figure 10. (a) Variation of potential and (b) mass changes of Pt electrode during the electrodeposition of EMD. applied anodic current density= $50 \mu A/cm^2$.

In order to investigate the effect of discharging-charging cycling on the air cathode, EMD was electrochemically deposited onto Pt substrate of electrochemical quartz crystal microbalance (EQCM). Fig. 10 shows that potential increases almost linearly with time and reaches a constant potential after 200 s. Simultaneous measurement of electrodeposited mass of MnO_2 increases constantly during deposition. Initial potential increase period during 200 s can be attributed to time needed to the full coverage of MnO_2 film on substrate Pt electrode. Total amount of $7.32 \mu g$ of EMD was deposited during 10 min, prior to the half cell test.

Figure 11 shows the variation of EMD electrode mass measured during potential cycling between 2.0V to 4.5V. Potential sweep to lower voltage can be interpreted as a cathodic discharging reaction and a reverse sweep is an anodic charging process of air cathode. Since discharging reaction is basically the formation reaction of Li_2CO_3 , $LiRCO_3$, Li_2O_2 compounds, it is expected that EMD electrode mass will be increased. During the first anodic sweep, it is supposed that the pre-deposited materials on EMD are detached and electrode mass decrease is observed. During the first discharging from 4.5 to 2.0V, mass increase Δm_{dis1} is $7.21 \mu g$.

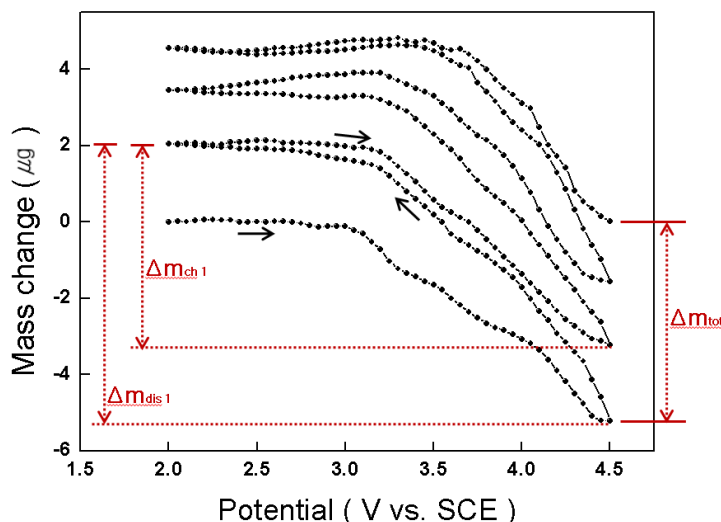


Figure 11. Mass changes of EMD during cyclic voltammetry in 1M LiPF₆ / PC:EC:DEC (1:4:5vol%) by using EQCM. Scan rate: 10 mV/s.

However, 72.5% of deposited discharging product (Δm_{ch1}) is removed during charging and the 30% of Δm_{dis1} , 1.98 µg is still remained onto EMD. When the cycling is reiterated 3 times, the deposited product is accumulated to Δm_{tot} , 5.2 µg. The accumulated deposits onto EMD will block the reaction sites and make difficult for oxygen to diffuse inside electrode and the discharge-charge capacity will be decreased. It will result in the decrease of three-phase boundary where discharging reaction takes place.

4. CONCLUSIONS

The performance of electrolyte manganese dioxide (EMD) as cathode active material for lithium-air battery was investigated in this work. Electrochemically prepared EMD is γ -phase and has a surface area of 37.4 m² g⁻¹. Electrochemical analysis indicated that KB containing 20wt% EMD electrode showed higher catalytic activity and specific capacity than KB only cathode. FT-IR and mass spectroscopy analysis suggested that lithium carbonates compounds were the main products formed during discharge and only a small amount of lithium oxides were produced. Since lithium carbonate compounds were produced from the dissociation of organic electrolyte, both the decrease of electrolyte amount and variation of electrolyte composition caused the deterioration of cell performance. Furthermore, surface analysis and electrochemical impedance spectroscopy supported that discharge products were not fully removed during charge process and, that is, discharge and charge reactions were only partially reversible. The accumulation of discharge reduction products on air cathode was quantitatively measured with EQCM. It resulted in the degradation of cycleability of lithium air battery by blocking the access of reactant oxygen and covering the reaction sites. Mechanism investigation of discharge and charge reaction should be elucidated to improve the cell performance and cycleability.

ACKNOWLEDGMENTS

This work was supported by the National Research Foundation of Korea Grant Funded by the Korean Government (MEST) (NRF-2012-M1A2A2671765).

References

1. K. M. Abraham, Z. Jiang, *J. Electrochem. Soc.*, 143 (1996) 1.
2. T. Ogasawara, A. Debart, M. Holzapfel, P. Novak, P. G. Bruce, *J. Am. Chem. Soc.*, 128 (2006) 1390.
3. J. Read, *J. Electrochem. Soc.*, 149 (2002) A1190.
4. A. Debart, A. J. Paterson, J. Bao, P. G. Bruce, *Angew. Chem.*, 120 (2008) 4597
5. L. Cecchetto, M. Salomon, and B. Scrosati, F. Croce, *J. Power Sources*, 213 (2012) 233
6. A. K. Thapa, B. Pandit, H. S. Paudei, R. Thapa, S. Ida, J. B. Jasinski, G.U. Sumanasekera, T. Ishihara, *Electrochim. Acta*, 127 (2014) 410
7. D. Zhang, Z. Fu, Z. Wei, T. Huang, A. Yu, *J. Electrochem. Soc.*, 157 (2010) A362
8. T. Kuboki, T. Okuyama, T. Ohsaki, N. Tamaki, *J. Power Sources*, 146 (2005) 766
9. C. W. Lee, K.W. Nam, B. W. Cho, K. B. Kim, *J. Microporous and Mesoporous Materials*, 130 (2010) A208
10. A. P. Malloy, G. J. Browning, S. W. Donne, *J. Colloid and Interface Science*. 285 (2005) A653
11. H. Adelhani, M. Ghaemi, *J. Allows and Compounds*, 481 (2009) 446
12. S. Devaraj, N. Munichandraiah, *Electrochem. Solid-state Lett.*, 12 (9) (2009) F21
13. S. D. Beattie, D. M. Manolescu, S. L. Blair, *J. Electrochem. Soc.*, 156 (2009) A44
14. H. Adelhani, *J. Electrochem. Soc.*, 156 (2009) A791
15. P. Yu, X. Zhang, Y. Chen, Y. Ma, Z. Qi, *Materials Chem. and Physics*, 118 (2009) 303
16. X. Fu, J. Feng, H. Wang, K. M. Ng, *J. Materials Research Bulletin*, 45 (2010) 1218
17. Q. Wei, X. Ren, J. Du, S. Wei, S. Hu, *J. Minerals Engineering*, 23 (2010) 578
18. J. E. Lewis, P. H. Scaife, D. A. J. Swinkels, *J. Applied Electrochem.*, 6 (1976) 199
19. K. R. Prasad, N. Miura, *J. Power Sources*, 135 (2004) 354
20. J. Read, *J. Electrochem. Soc.*, 153 (2006) A96
21. J. Read, K. Mutolo, M. Ervin, W. Behl, J. Wolfenstein, A. Drieger, D. Foster, *J. Electrochem. Soc.*, 150 (2003) A1351
22. X. Ren, SS Zhang, D. T. Tran, *J. Mater. Chem.*, 21 (2011) 10118
23. S. A. Freunberger, T. Chen, N. E. Drewett, *Angewante Chem.*, 50 (2011) 1
24. F. Mizuno, H. Iba, 219th ECS meeting. Abst. #401, 2011
25. S. A. Freunberger, Y. Chen, Z. Peng, J. M. Griffin, L. J. Hardwick, F. Bard, P. Novak, P. G. Bruce, *J. Am. Chem. Soc.*, 133 (2011) 8040
26. W. Xu, V. V. Viswanathan, D. Wang, S. A. Towne, J. Xiao, Z. Nie, D. Hu, J. G. Zhang, *J. Power Sources*, 196 (2011) 3894
27. J. Xiao, J. Hu, D. Wang, D. Hu, W. Xu, G. L. Graff, Z. Nie, J. Liu, J. G. Zhang, *J. Power Sources*, 196 (2011) 5674
28. M. Mirzaeian, P. J. Hall, *J. Power Sources*, 195 (2010) 6817
29. H. Chen, K. Scott, *J. Power Sources*, 195 (2010) 1370
30. N. Ominde, X.-Q. Yang, D. Qu, 215th ECS Meeting, Abst. #240, (2009).
31. F. Mizuno, S. Nakanishi, Y. Lotani, S. Yokoishi, H. Iba, *Electrochem. Comm.*, 78 (2010) 403